Available online at www.sciencedirect.com
ScienceDirect
Geochimica et Cosmochimica Acta 73 (2009) 3642–3655
Geochimica et Cosmochimica Acta
www.elsevier.com/locate/gca

Water diffusion in dacitic melt

Huaiwei Ni [a,*], Harald Behrens [b], Youxue Zhang [a]

[a] Department of Geological Sciences, The University of Michigan, Ann Arbor, MI 48109-1005, USA
[b] Institut für Mineralogie, UNI Hannover, Callinstr. 3, D-30167 Hannover, Germany

Received 6 October 2008; accepted in revised form 23 March 2009; available online 2 April 2009

Abstract

H_2O diffusion in dacitic melt was investigated at 0.48–0.95 GPa and 786–893 K in a piston-cylinder apparatus. The diffusion couple design was used, in which a nominally dry dacitic glass makes one half and is juxtaposed with a hydrous dacitic glass containing up to ~8 wt.% total water (H_2O_t). H_2O concentration profiles were measured on quenched glasses with infrared microspectroscopy. The H_2O diffusivity in dacite increases rapidly with water content under experimental conditions, similar to previous measurements at the same temperature but at pressure <0.15 GPa. However, compared with the low-pressure data, H_2O diffusion at high pressure is systematically slower. H_2O diffusion profiles in dacite can be modeled by assuming molecular H_2O (H_2O_m) is the diffusing species. Total H_2O diffusivity $D_{H_2O_t}$ within 786–1798 K, 0–1 GPa, and 0–8 wt.% H_2O_t can be expressed as: $D_{H_2O_t} = \left[1 + \frac{2X-1}{\sqrt{4X(X-1)(1-4/K)+1}}\right] \exp\left(-9.423 - 62.38X - \frac{19064-108882X+1476.7P}{T}\right)$, where $D_{H_2O_t}$ is in m^2/s, T is temperature in K, P is pressure in GPa, $K = \exp(1.49 - 2634/T)$ is the equilibrium constant of speciation reaction ($H_2O_m + O \rightleftharpoons 2OH$) in the melt, $X = C/18.015/[C/18.015 + (100 - C)/33.82]$, C is wt.% of H_2O_t, and 18.015 and 33.82 g/mol correspond to the molar masses of H_2O and anhydrous dacite on a single oxygen basis. Compared to H_2O diffusion in rhyolite, diffusivity in dacite is lower at intermediate temperatures but higher at superliquidus temperatures. This general H_2O diffusivity expression can be applied to a broad range of geological conditions, including both magma chamber processes and volcanic eruption dynamics from conduit to the surface.

1. INTRODUCTION

Water diffusion in natural silicate melts has been extensively studied due to its importance in a variety of magmatic and volcanic processes (Zhang et al., 2007). For example, through diffusive transport of water, bubbles in magma can extract water from magma as nutrient for growth (e.g., Proussevitch and Sahagian, 1998; Liu and Zhang, 2000). Other relevant circumstances include magma dehydration and fragmentation (e.g., Zhang, 1999; Martel et al., 2000). Furthermore, water diffusion could also play an important role in deep-seated magma reservoir processes, such as the interaction between two melts or between a fluid and a melt.

Reported water diffusivity data has covered diverse melt compositions, including "normal" metaluminous rhyolite (e.g., Shaw, 1974; Delaney and Karsten, 1981; Zhang et al., 1991; Nowak and Behrens, 1997; Zhang and Behrens, 2000; Okumura and Nakashima, 2004; Behrens et al., 2007; Ni and Zhang, 2008), peralkaline rhyolite (Behrens and Zhang, 2009; Wang et al., 2009), dacite (Liu et al., 2004a; Behrens et al., 2004; Okumura and Nakashima, 2006), andesite (Behrens et al., 2004; Okumura and Nakashima, 2006; Ni et al., 2009), basalt (Zhang and Stolper, 1991; Okumura and Nakashima, 2006), and trachyte (Freda et al., 2003). These contributions have established that the diffusivity of H_2O depends on temperature, pressure, water content, and chemical composition of the melt. However, a

* Corresponding author. Address: Department of Geological Sciences, The University of Michigan, 2534 C. C. Little, 1100 North University Ave., Ann Arbor, MI 48109-1005, USA. Fax: +1 734 763 4690.
E-mail address: hni@umich.edu (H. Ni).

0016-7037/$ - see front matter © 2009 Elsevier Ltd. All rights reserved.
doi:10.1016/j.gca.2009.03.029

general H_2O diffusivity expression that is applicable to a broad range of geological conditions is only available for rhyolite (Ni and Zhang, 2008). For other melts, *T*- and *P*-dependences of H_2O diffusivity cannot be well constrained because there are no data at high pressures and intermediate temperatures (773–973 K). The absence of a general expression to predict H_2O diffusivity in dacitic melt makes it difficult to simulate the dynamics of volcanic eruptions.

Many arc volcanic eruptions have a dacitic bulk composition, such as the 1980 eruption of Mount St. Helens (Fruchter et al., 1980) and the 1991 eruption of Mount Unzen (Chen et al., 1993), although the composition of the residual melt is more silicic. There are andesitic eruptions with dacitic liquid composition as well, such as the 1968 eruption of Arenal Volcano (Szramek et al., 2006). Several experimental studies have been carried out on water diffusion in dacite. At high pressures (0.5–1.5 GPa) and superliquidus high temperatures (1458–1798 K), Behrens et al. (2004) measured H_2O diffusivity (up to 6 wt.% H_2O) using a diffusion-couple technique. They showed that H_2O diffusivity is roughly proportional to water content, and pressure effect at such high temperatures is small. Liu et al. (2004a) investigated the dehydration rate of hydrous dacitic glass containing 0.7–2.5 wt.% H_2O at 824–911 K and 0.1–145 MPa. Water diffusivity in dacite was found to increase with water content, more rapidly than in rhyolite, and more rapidly than the proportionality relation as H_2O_t is greater than 1 wt% at such temperatures. Under similar conditions (773–948 K and room pressure), Okumura and Nakashima (2006) conducted in situ measurements on the bulk water content of hydrous dacitic glasses, and adopted a proportional correlation between diffusivity and water content (<1 wt.%).

Because previous experiments on H_2O diffusion in dacitic melts cover either intermediate temperature and low pressure (773–948 K, 0.1–145 MPa), or high temperature and high pressure (1458–1798 K, 0.5–1.5 GPa), the temperature effect (or the pressure effect depending on which parameters one is interested in) is not well established. Zhang et al. (2007) ignored the pressure effect to combine the high and low temperature data. Furthermore, the data at intermediate temperatures only cover low H_2O concentration (up to 2.5 wt.%). In order to elucidate the pressure influence on H_2O diffusivity in dacite and to further constrain how H_2O diffusivity depends on a wide range of H_2O content, temperature, and pressure, we have performed diffusion-couple experiments at 786–893 K and 0.48–0.95 GPa in a piston-cylinder apparatus. The acquired diffusivity data in this work and those from previous studies allow construction of a general expression of H_2O diffusivity in dacitic melt, which can be applied to most geological circumstances.

2. EXPERIMENTAL AND ANALYTICAL PROCEDURES

2.1. Starting material

The diffusion couple is composed of a nominally anhydrous and a hydrous dacitic glass. The anhydrous dacite was produced by melting oxides and carbonates at 1873 K, and hydrous glasses were synthesized at 0.5 GPa and 1523–1623 K for 1–2 days in an internally heated pressure vessel at University of Hannover, Germany. The method of synthesis was described in detail in Ohlhorst et al. (2001) and Behrens et al. (2004). No crystals or bubbles were observed in all the run products. The nominally anhydrous glass contains 0.013 wt.% water (Table 1). Several pieces of hydrous glasses were prepared with 1.4–7.9 wt.% H_2O based on FTIR analyses, and the relative variation within each sample is less than 5%. All dacitic glasses were analyzed with a Cameca SX100 electron microprobe at the University of Michigan, and their anhydrous compositions are reported in Table 1. The compositions are close to the bulk rock products of the 1980 Mount St. Helens (Fruchter et al., 1980), the 1991 Pinatubo (Bernard et al., 1991), and the 1991 Unzen dacitic eruptions (Chen et al., 1993), and are also similar to samples used in previous H_2O diffusion studies (Liu et al., 2004a; Behrens et al., 2004; Okumura and Nakashima, 2006).

Table 1
Composition of starting dacitic glass (in wt.%) on anhydrous basis[a].

	DRY-DC	DC1.4	Dac4	Dac5	Dac8
SiO_2	65.41	66.35	66.60	67.30	65.46
TiO_2	0.87	0.63	0.80	0.76	0.63
Al_2O_3	15.73	16.58	14.91	15.23	16.05
FeO_T	4.43	3.73	4.87	4.36	4.50
MnO	0.08	0.07	0.05	0.08	0.05
MgO	1.95	1.85	2.22	2.13	2.19
CaO	4.90	4.70	4.92	4.72	4.89
Na_2O	4.00	4.05	3.48	3.57	3.84
K_2O	2.51	2.72	2.51	2.44	2.55
Total	99.88	100.68	100.36	100.59	100.16
H_2O (IR)	0.013	1.42	4.91	5.49	7.85

[a] A Cameca SX100 electron microprobe is used to make 5 analyses on each sample, with a scanning beam (5 μm by 5 μm) of 15 kV voltage and 4 nA current. Oxide contents are reported on anhydrous basis: raw oxide contents divided by $(1 - C/100)$ with C being water content in wt.%. Water content was measured with infrared spectrometry based on the calibration by Yamashita et al. (1997) for DRY-DC and that by Ohlhorst et al. (2001) for the hydrous glasses.

2.2. Diffusion runs

Diffusion runs were performed in a 0.5″ end-loaded piston cylinder apparatus at the University of Michigan. Considering the positive correlation between water diffusivity and water content, we always adopted a longer hydrous glass cylinder (2.6–3.0 mm length) than the anhydrous one (1.0–1.7 mm length) for the two halves of a diffusion couple. The cylinder pair of ~2.6 mm diameter was first placed in a graphite capsule of 4.5 mm outer diameter, with their polished surface in direct contact. The graphite capsule was then enclosed in a gold tube of 5 mm outer diameter and 0.2 mm wall thickness, which was welded on both ends. To ensure that convection does not contribute to the exchange of water, the capsule was always oriented to keep

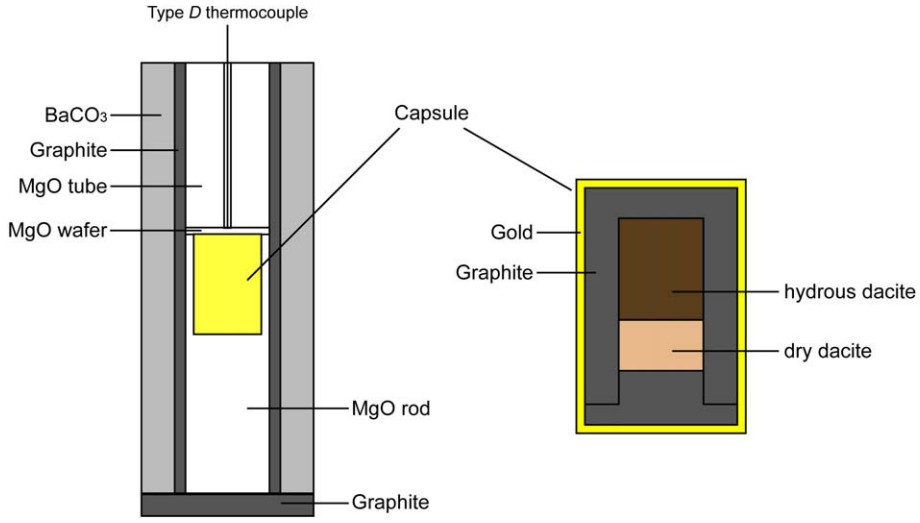

Fig. 1. Sketches of sample assemblage and capsule for the 0.5″ piston cylinder apparatus used in this study. The outside diameter of gold capsule is 5 mm.

the hydrous half on top when placed into a crushable MgO rod. Outside the MgO rod was a graphite heater and then a $BaCO_3$ cell, together forming the entire sample assemblage (Fig. 1).

The temperature during diffusion runs was measured by a type D thermocouple (Re_3W_{97}–$Re_{25}W_{75}$), which was separated from the gold capsule by an MgO wafer of 0.5 mm thickness. The calibrated temperature profile of the experimental charge (Hui et al., 2008) indicates that a temperature-dependent correction should be made in order to find the real temperature at the center of the charge (also the center of the dacite samples). The temperature correction is 13–20 K for the reported runs. After taking into account uncertainties in thermocouple and sample position and temperature fluctuation (typically within ±2 K), the overall 2σ error in temperature is estimated of about 10 K.

Experiments were carried out at 0.5 and 1 GPa (nominal pressure) with a "piston-out" procedure. Real pressure of our piston cylinder is 5–6% lower than nominal pressure (Hui et al., 2008; Ni and Zhang, 2008), and pressure correction is made accordingly. Due to imperfect pressure calibration as well as gauge imprecision and pressure fluctuation, the overall pressure uncertainty is approximately 50 MPa. To extend the pressure coverage, an experiment was conducted at 2 GPa and 873 K. However, the hydrous half crystallized, consistent with previous observations that increasing pressure increases the likelihood of crystallization (Hui et al., 2008; Ni and Zhang, 2008; Wang et al., 2009). Hence, no further experiments were conducted at >1 GPa.

Diffusion runs were initiated either by programmed stepwise heating (reaching target temperature in <30 s) or by manual heating (reaching target T in a couple of minutes) from the relaxation temperature of 373 K. The experimental duration spanned 0.5–136 h, depending on temperature and maximum water content. Experiments were ended by turning off the heating power, and the initial cooling rate was roughly 80 K/s based on recorded thermal history.

Table 2
Experimental conditions.

Run #	H_2O_t (I)[a](wt.%)	T[b](K)	P[c] (GPa)	t (s)	H_2O_t (E)[d] (wt.%)	Thickness (μm)
Dac-DC05-12	0.01/7.9	893 ± 10	0.95 ± 0.05	1825	0.01/7.7	264
Dac-DC05-13	0.01/5.5	892 ± 10	0.95 ± 0.05	54,000	0.01/5.3	203
Dac-DC05-14	0.01/7.9	840 ± 10	0.95 ± 0.05	10,800	0.01/7.7	215
Dac-DC06-15	0.01/5.5	842 ± 10	0.95 ± 0.05	144,000	0.01/5.7	191
Dac-DC06-17[e,f]	0.01/7.9	786 ± 10	0.95 ± 0.05	175,780	0.01/6.7	205
Dac-DC06-19[f]	0.01/4.9	893 ± 10	0.48 ± 0.05	185,400	0.01/4.0	206
Dac-DC06-21	0.01/1.4	842 ± 10	0.95 ± 0.05	489,600	0.01/1.4	173
Dac-DC06-22	0.01/5.5	791 ± 10	0.95 ± 0.05	252,000	0.02/5.8	157

[a] Initial water contents of the two halves measured by FTIR based on the calibration of Yamashita et al. (1997) and Ohlhorst et al. (2001).
[b] Effective temperature after considering axial thermal gradient in piston-cylinder apparatus (13–20 K).
[c] Effective pressure based on measured quartz-coesite transition against the phase boundary determined by Bose and Ganguly (1995).
[d] End minimum and maximum water contents measured at the flat regions of each diffusion profile. Nominal H_2O concentration is divided by a factor of 1.144 to account for baseline change in IR spectra after run.
[e] Heating power was disconnected after a duration of ~50 min and the capsule was reused.
[f] Long dwelling time caused noticeable water loss in the hydrous half.

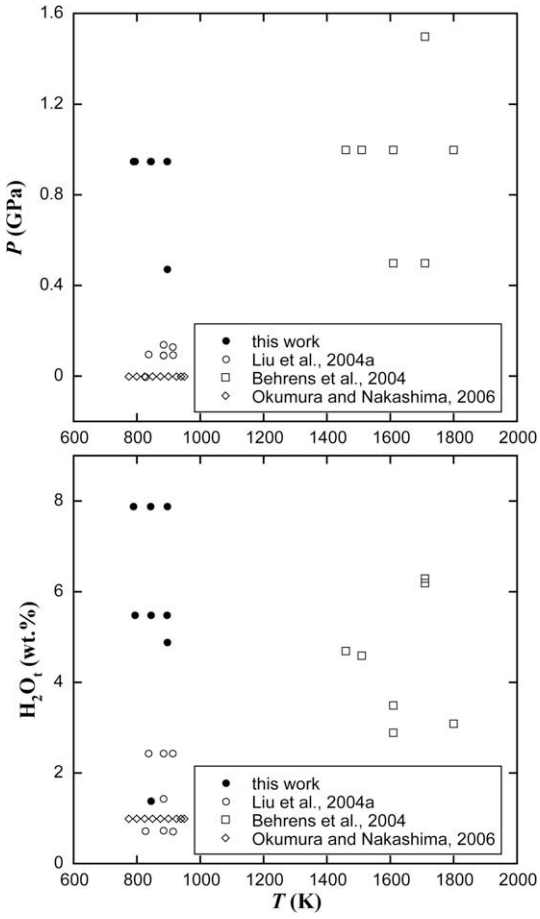

Fig. 2. Experimental conditions of this work and previous studies on H_2O diffusion in dacite: Liu et al. (2004a), Behrens et al. (2004), and Okumura and Nakashima (2006).

Table 2 lists the details of experimental conditions. These experiments occupy the T-P-H_2O wt.% space not covered by previous works on dacite (Liu et al., 2004a; Behrens et al., 2004; Okumura and Nakashima, 2006), as displayed in Fig. 2, and they are necessary for resolving the dependence of H_2O diffusivity on pressure and H_2O_t, and hence for a quantitative understanding of how H_2O diffusivity depends on various controlling factors.

2.3. FTIR analyses

Infrared analyses on doubly polished dacite glass wafers were performed at the University of Michigan using a Perkin-Elmer Spectrum GX FTIR spectrometer. Before diffusion experiments, bulk water contents in dacite wafers (Table 1) were analyzed using the FTIR with a NIR source, a CaF_2 beamsplitter, and an InSb detector cooled by liquid nitrogen. Infrared spectra were collected from 2000 to 9000 cm^{-1} wave numbers and 64–128 scans were accumulated for each analysis. The 3550 cm^{-1} MIR absorption band calibrated by Yamashita et al. (1997) was applied to calculate the extremely low H_2O concentration in the nominally anhydrous dacite glass. For hydrous glasses, NIR bands at 5200 cm^{-1} (signifying H_2O molecules, or H_2O_m) and 4500 cm^{-1} (signifying hydroxyl group, or OH) were used to obtain the total water (H_2O_t) content ($H_2O_m + OH$) with the calibration by Ohlhorst et al. (2001). TT baselines (TT stands for two-tangential or tangential-tangential, Withers and Behrens, 1999) were used to determine absorption peak heights for all spectra. Typical tangential points are located approximately at 4250 and 4650 cm^{-1} for the 4500 cm^{-1} OH band, and located at ~4700 and ~5400 cm^{-1} for the 5200 cm^{-1} H_2O_m band. However, the tangential point at ~5400 cm^{-1} may not be well defined in the presence of iron-related bands (Ohlhorst et al., 2001).

Each quenched capsule after a diffusion experimental run was mounted into epoxy resin and polished to reveal a central section of 160–260 μm thickness. No sign of crystallization in glass was observed under optical microscope for the reported runs. Typically one curved crack (roughly perpendicular to the cylinder axis) was developed in the glass, likely formed during the rapid quenching. As the crack often lies outside the effective diffusion profile, it does not cause much problem in diffusivity determinations.

The post-experimental diffusion profiles were analyzed using the AutoImage microscope system (with an MCT detector) on the Perkin-Elmer Spectrum GX FTIR spectrometer. The aperture was 10 μm wide and 200 μm long on the focus plane of the microscope. However, the real spatial resolution is larger than the aperture width. For example, the measurement of a step concentration profile yields a full width at half maximum (FWHM) of 30 μm (Ni and Zhang, 2008) for the case of a 20-μm wide aperture. The FWHM of 10-μm wide aperture is determined to be ~15 μm. Such spatial resolution is tolerable for most diffusion profiles, which are more than 300 μm long. Measured profiles change little upon further polishing. For two short profiles (with profile length <240 μm), Dac-DC05-12 and Dac-DC06-21, convolution effect may play a significant role, which will be discussed later. The IR spectra along diffusion profiles were collected and handled using a procedure similar to that used for the IR analysis of the starting materials.

3. RESULTS

Diffusion profiles have been successfully acquired for eight experiments, whereas other runs failed due to power breakage or crystallization or poor contact between the diffusion halves. For experiment Dac-DC06-17, power was shut down after a sudden temperature rise (~5 K) was noticed (when the dwelling time is roughly 1 h), and the capsule was taken out and reused for a second run. In consideration of its long dwelling time, duration correction due to extra cooling and heating is negligible. The detailed experimental conditions are summarized in Table 2, and the measured H_2O_t concentration profiles are plotted with curve fits in Fig. 3. The species concentrations (H_2O_m and OH) are not used for modeling diffusivity because (a) they are less accurate than H_2O_t concentration (Ohlhorst et al., 2001); and (b) they may not represent equilibrium speciation at experimental conditions, especially at high H_2O_t.

As observed by Liu et al. (2004a) and Behrens et al. (2004), water content by NIR analysis often shows a

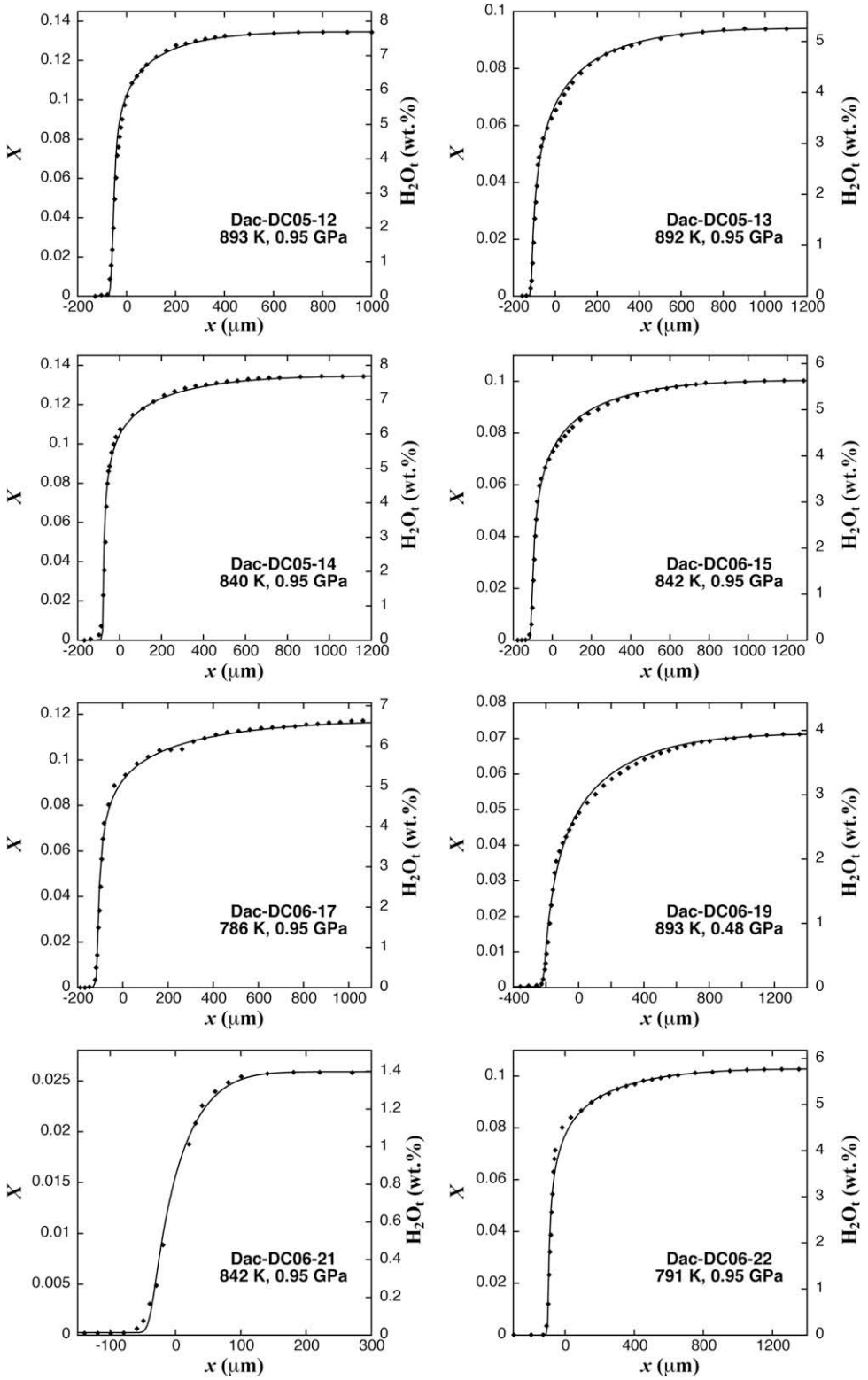

Fig. 3. H_2O_t concentration profiles in the diffusion-couples, with some data points outside the illustrated distance range for clarity. x is arbitrary distance but close to the original interface. Fitting curves are also shown for comparison based on the model of $D_{H_2O_m} = D_0\exp[(-62.38 + 108882/T)X]$, with results reported as $\ln D_0$ in Table 5. Convolution effect is considered for the short profile of Dac-DC05-12 and Dac-DC06-21. See text for details.

Table 3
Ferrous iron quantification before (I) and after (E) heating and pressurization at 0.95 GPa[a].

Run #	T (K)	H_2O (wt.%)	Fe^{2+}/Fe_{tot} (I)	Fe^{2+}/Fe_{tot} (E)
Dac-DC05-08	873	0.01	0.397 ± 0.017	0.453 ± 0.064
		1.1	0.796 ± 0.021	0.812 ± 0.030
Dac-DC05-10	873	0.01	0.389 ± 0.014	0.432 ± 0.046
		3.5	0.621 ± 0.018	0.649 ± 0.038
Dac-sp1	753	7.9	0.66 ± 0.03	0.70 ± 0.02

[a] The colorimetric method by Schuessler et al. (2008) was used and analyses results are reported with 2σ error.

nominal increase of about 10–20% after diffusion runs. One might expect this effect is related to the change in redox state of iron ($Fe_2O_3 + H_2 \rightleftharpoons 2FeO + H_2O$) in the presence of the graphite capsule. However, Fe^{2+}/Fe_{tot} analyses on glasses before and after diffusion runs using a colorimetric technique (Schuessler et al., 2008) show only minor increase in ferrous iron (Table 3), which is equivalent to no more than 0.03 wt% H_2O_t increase. Furthermore, Behrens et al. (2004) demonstrated that redox state of iron has little influence on H_2O diffusion at high temperatures (>1573 K) even in high-iron andesite (containing 7–8 wt.% FeO_t). For our experiments in dacite containing 4–5 wt% FeO_t, we expect that the influence of small change in Fe redox state is insignificant. Therefore, elevated nominal H_2O concentration is an artifact, possibly caused by the effect on the band intensity and baseline of IR spectra (Liu et al., 2004a; Fig. 4) due to factors such as changing Fe^{2+} coordination or formation of nanocrystals (Liebske et al., 2003). Accordingly, nominal H_2O concentrations in diffusion profiles determined by NIR are divided by an averaged factor of 1.144 to be consistent with initial H_2O concentrations. This factor is also applied to the profiles of Liu et al. (2004a) and Behrens et al. (2004) in the presence of IR baseline change and nominal H_2O increase when their data are discussed below.

Experimental durations have been designed so that large regions maintain initial water contents in both halves (meaning that diffusion in infinite medium applies). However, Dac-DC06-17 and Dac-DC06-19 show evident water loss in the hydrous half, which causes extra uncertainty in determining H_2O diffusivity.

Water can also be lost from the cylindrical sides during the high-temperature experiments. The size of the samples is designed so that for a region near the centerline (~800 μm diameter), water loss from the sides is negligible. Fig. 5 shows two radial concentration distributions. There is indeed water loss from the sides. Most of our samples are similar to Dac-DC06-22 in Fig. 5 with a flat center region, except for Dac-DC06-17 and Dac-DC06-19. Because the measured concentration profiles are along and near the centerline where water loss from the sides can be ignored, they can be treated as one-dimensional diffusion. The two samples Dac-DC06-17 and Dac-DC06-19 that show water loss from the centerline are more complicated. When the data are modeled, results from these two samples are carefully checked for possible inconsistency with other experiments. In the end, the results from these two experiments are still roughly consistent with other experiments within uncertainty.

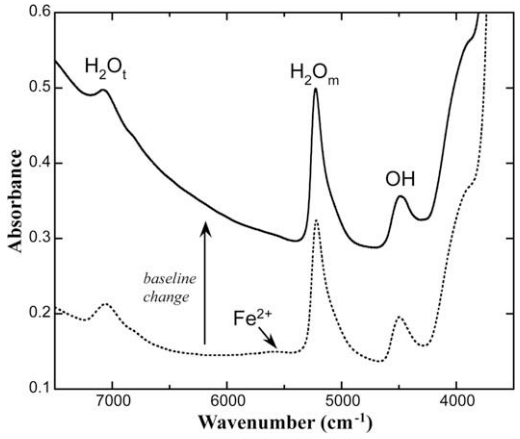

Fig. 4. NIR absorption bands of Dac8 (dash curve) become stronger after diffusion run Dac-DC05-12 (solid curve), presumably due to the change of Fe^{2+} coordination or even formation of nanocrystals. The baseline also becomes steeper above 5400 cm^{-1}.

4. DISCUSSION AND APPLICATION

4.1. Diffusion mechanism and modeling

Following previous workers (Zhang and Behrens, 2000; Liu et al., 2004a; Ni and Zhang, 2008), H_2O diffusion in silicate melts is treated as follows:

$$\frac{\partial X}{\partial t} = \frac{\partial}{\partial x}\left(D_{H_2O_m}\frac{\partial X_m}{\partial x}\right). \quad (1)$$

Here X is the mole fraction of total dissolved H_2O, and is related to H_2O percentage (C in wt.%) through $X = C/18.015/[C/18.015+(100 - C)/33.82]$, where 18.015 and

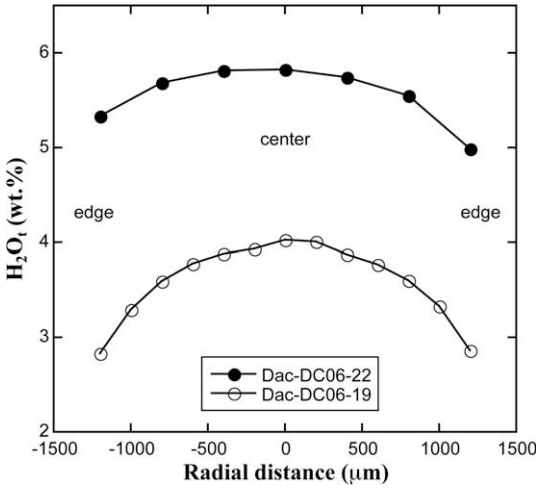

Fig. 5. Radial distribution of water content in the hydrous half of two diffusion experiments (the center of each sample is defined as zero distance). Water loss from the edge of sample is evident in both cases. But in Dac-DC06-22, a plateau within ~400 μm around the centerline maintains the initial water content; whereas in Dac-DC06-19, there is no plateau and even the center suffered from water loss.

33.82 g/mol are the molar masses of H_2O and anhydrous dacite on a single oxygen basis, respectively. X_m is the mole fraction of H_2O_m, t is time, x is distance, and $D_{H_2O_m}$ is H_2O_m diffusivity.

Despite the sluggishness of OH diffusion, the concentration of OH still varies with time in response to the change in H_2O_m concentration through the reaction ($H_2O_m + O \rightleftharpoons 2OH$), in order to maintain equilibrium. The equilibrium constant K of this speciation reaction in dacite was reported by Liu et al. (2004b) using two different IR baselines (TT and GG). We choose the TT expression of K in this work because (a) tangential baselines were adopted for water concentration determination in this study; (b) K from the TT method lies between that of rhyolite (Zhang et al., 1997) and that of andesite (Botcharnikov et al., 2006; Ni et al., 2009), which agrees with the observation that K decreases with silica content (Silver et al., 1990) and increases with NBO/T (and decreasing content of alkali earth elements) (Behrens and Yamashita, 2008). Hence equilibrium constant K in dacite is assumed to be dependent on temperature as follows (Liu et al., 2004b):

$$\ln K = 1.49 - \frac{2634}{T}, \quad (2)$$

where T is in K. The pressure dependence of water speciation has been shown to be minimal from 0 to 1 GPa in rhyolitic melt (Hui et al., 2008). Furthermore, one should note that the choice of the equation for water speciation affects the derived molecular H_2O diffusivity but has only negligible influence on the derived total H_2O diffusivity, and the latter is critical in calculating diffusion profiles.

H_2O_m diffusivity has been shown to increase rapidly with water content in rhyolite and dacite, especially at low temperatures such as 823 K (Zhang and Behrens, 2000; Liu et al., 2004a; Ni and Zhang, 2008), which led to the exponential relationship:

$$D_{H_2O_m} = D_0 \exp(aX), \quad (3)$$

where D_0 and a are both constants at given T and P. Watson (1991) and Behrens and Zhang (2001) have described similar dependence on water content for diffusivity of neutral particles such as CO_2 molecules and Ar atoms in rhyolitic melts.

Eqs. (2) and (3) are used to numerically solve the governing equation of H_2O diffusion (Eq. (1)) and model the measured diffusion profiles. First we need to constrain parameter a. In this work multiple experiments have been carried out at the same T and P with samples containing different H_2O concentrations. If they can be fit well with the same combination of D_0 and a, that is a good indication of model validity. This criterion has been successfully applied to the diffusion profiles at 0.95 GPa and three temperatures (Table 4), with the relative error of a estimated about 7% (e.g., 68 ± 5 at 841 K). Fitting results show that a increases as temperature decreases, as also observed from

Table 4
Best-fit a values using the model $D_{H_2O_m} = D_0 \exp(aX)$ and $\ln K = 1.49 - 2634/T$.

Run #	T (K)	P (GPa)	a	R^2
Dac-DC05-12	~893	0.95	62 ± 5	0.9928
Dac-DC05-13				0.9976
Dac-DC05-14	~841	0.95	68 ± 5	0.9972
Dac-DC06-15				0.9978
Dac-DC06-17	~789	0.95	72 ± 5	0.9941
Dac-DC06-22				0.9965
Refit from Liu et al. (2004a)				
DC2B5	~911	~0.11	52 ± 5	0.9983
DC53b2				0.9988
DC2B4	881	~0.11	66 ± 5	0.9973
DC1				0.9951
DC53b1				0.9979
Refit from Behrens et al. (2004)				
DacDC6	1798	1.0	-8.6 ± 12.3	0.9909
DacDC3	1708	0.5	-0.4 ± 4.7	0.9954
			0.2 ± 5.0	0.9961
DacDC2	1608	1.0	7.1 ± 10.0	0.9950
DacDC5	1508	1.0	10.9 ± 5.1	0.9966
DacDC7	1458	1.0	17.2 ± 6.0	0.9972

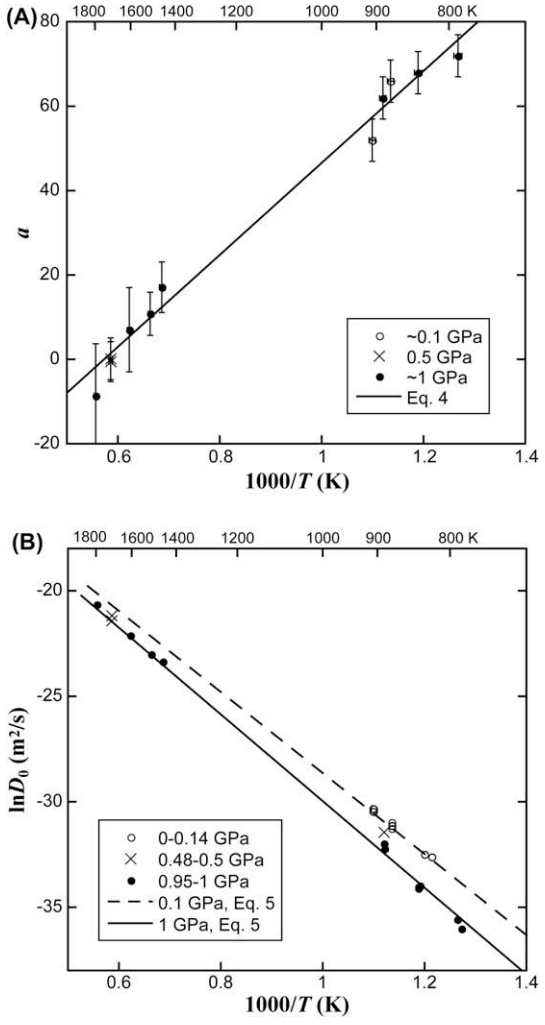

Fig. 6. Best-fit parameters using the model $D_{H_2O_m} = D_0 \exp(aX)$. (A) Parameter a from this work and from refits of data in Liu et al. (2004a) and Behrens et al. (2004). (B) ln D_0 (Table 5) at various T and P assuming Eq. (4), indicating progressively negative pressure effect towards low T. Also shown are calculated ln D_0 at 0.1 GPa (dash line) and 1 GPa (solid line) from Eq. (5).

the dehydration profiles of Liu et al. (2004a) and for rhyolitic melt (Ni and Zhang, 2008). The diffusion profiles from Behrens et al. (2004) were also refit to constrain parameter a in high temperature range, with a program allowing multivariate (D_0 and a) fitting and error analysis for a single profile (Ni and Zhang, 2008). The dependence of H_2O_m diffusivity on water content turns out to be much smaller at high temperatures, and in some cases (above 1750 K) even negative a values are found from fitting. Because these temperatures are beyond typical magmatic temperatures and the negative values of a are within uncertainty of zero, we did not experimentally explore further the validity of the negative a values. The results of best-fit parameter a are summarized in Table 4 and are plotted in Fig. 6A, and they roughly form a linear trend with $1000/T$ (with little pressure dependence), which can be fit (York, 1966) as

$$a = (-62.380 \pm 5.851) + \frac{108882 \pm 6185}{T}, \quad (4)$$

where T is in K. By assuming Eq. (4), all diffusion profiles from Liu et al. (2004a), Behrens et al. (2004) and this work are fit again to constrain parameter D_0. Because the profiles of Dac-DC05-12 and Dac-DC06-21 are rather short (240 and 130 μm, respectively), they may have been considerably influenced by convolution effect (measured composition reflects the weighted average composition around the point of analysis, Ganguly et al., 1988). Therefore, a convoluted profile is first computed by assuming that the spatial resolution of IR measurement is roughly 15 μm, and then the new profile is used for fitting to find D_0.

The resulting D_0 values are reported in Table 5 and plotted in Fig. 6B. Furthermore, fitting curves have been compared with measured profiles in Fig. 3, showing good matches. Although a pressure effect cannot be easily resolved in the high temperature range, at lower T, D_0 does show a systematic decrease from <0.15 to ~1 GPa. The pressure dependence indicates a positive activation volume for H_2O_m diffusion. The dependence of D_0 on T and P can be characterized as follows:

$$D_0 = \exp\left[(-9.423 \pm 0.351) - \frac{(19064 \pm 303) + (1476.7 \pm 218.5)P}{T}\right] \quad (5)$$

where D_0 is in m^2/s, T is in K, and P is in GPa. This regression reproduces most experimental $\ln D_0$ values to within 0.4 (or a factor of 1.5 for D_0). The calculated dependence of $\ln D_0$ on temperature from Eq. (5) is illustrated at 0.1 GPa (dash line) and 1 GPa (solid line) in Fig. 6B. The calculated activation energy E_a based on the above expression is 159 kJ/mol at zero pressure. The activation volume $\Delta V^{\ddagger}$ in dacitic melt is $12 \pm 2\ cm^3/mol$ (the temperature dependence of $\Delta V^{\ddagger}$ cannot be resolved), whereas that for

Table 5
Fitting results of all H_2O diffusion profiles in dacite assuming $D_{H_2O_m} = D_0 \exp[(-62.38 + 108882/T)X]$.

Run #	T (K)	P (GPa)	H_2O_t (wt.%)	ln D_0 (m^2/s)	R^2	Source
Diffusion-couple						
DacDC6	1798	1.0	2.7	–20.63±0.12	0.9906	2
DacDC3	1708	0.5	5.4	–21.16±0.08	0.9953	2
				–21.40±0.09	0.9961	2
DacDC2	1608	1.0	2.6	–22.10±0.10	0.9950	2
DacDC5	1508	1.0	4.0	–23.00±0.08	0.9966	2
DacDC7	1458	1.0	4.1	–23.34±0.08	0.9970	2
Dac-DC05-12*	893	0.95	7.7	–31.96±0.04	0.9937	3
Dac-DC06-19	893	0.48	4.0	–31.42±0.08	0.9978	3
Dac-DC05-13	892	0.95	5.3	–32.21±0.10	0.9973	3
Dac-DC06-15	842	0.95	5.7	–34.08±0.09	0.9982	3
Dac-DC06-21*	842	0.95	1.4	–34.01±0.14	0.9982	3
Dac-DC05-14	840	0.95	7.7	–33.96±0.25	0.9936	3
Dac-DC06-22	791	0.95	5.8	–35.56±0.21	0.9958	3
Dac-DC06-17	786	0.95	6.7	–36.00±0.20	0.9950	3
Dehydration						
DC53b2	911	0.097	0.8	–30.43±0.06	0.9976	1
				–30.29±0.05	0.9987	1
DC2B5	910	0.133	2.6	–30.44±0.06	0.9978	1
				–30.31±0.07	0.9972	1
DC53b1	881	0.095	0.8	–31.24±0.05	0.9979	1
				–31.11±0.07	0.9974	1
DC1	881	0.096	1.5	–31.09±0.08	0.9956	1
DC2B4	881	0.143	2.5	–30.96±0.06	0.9979	1
DC2A3	834	0.100	2.4	–32.46±0.06	0.9970	1
				–32.47±0.08	0.9950	1
DC53b3	824	0.0001	0.8	–32.59±0.03	0.9994	1
				–32.58±0.08	0.9964	1

R^2 is the multiple correlation coefficient of each concentration profile fit. Source of data: [1], Liu et al. (2004a); [2], Behrens et al. (2004); [3], this work.
*Fit with convoluted theoretical profile (see text).

H_2O diffusion in rhyolitic melt is about 25 cm^3/mol at 330 K and about 10 cm^3/mol at 1283 K. H_2O_m diffusivity at a given T, P, and X can be calculated by combining Eqs. (3)–(5):

$$D_{H_2O_m} = \exp\left(-9.423 - 62.38X - \frac{19064 - 108882X + 1476.7P}{T}\right). \quad (6)$$

4.2. $D_{H_2O_t}$ and T-P-X dependence

H_2O_t diffusivity can be calculated from H_2O_m diffusivity through

$$D_{H_2O_t} = D_{H_2O_m}\frac{dX_m}{dX}, \quad (7)$$

Where $D_{H_2O_m}$ is from Eq. (6), and dX_m/dX depends on equilibrium constant of the speciation reaction (Eq. (2)) and H_2O_t mole fraction X, leading to (Wang et al., 2009):

$$D_{H_2O_t} = D_{H_2O_m}\left[1 + \frac{2X - 1}{\sqrt{4X(X-1)(1-4/K)+1}}\right]. \quad (8)$$

The above expression to calculate $D_{H_2O_t}$ reproduces all diffusion data (Liu et al., 2004a; Behrens et al., 2004; and this work) well and to almost the same precision as the diffusivity expressions of Liu et al. (2004a) and Behrens et al. (2004) specific for limited T-P-H_2O_t conditions. Hence, the above expression supersedes the previous expressions in Liu et al. (2004a), Behrens et al. (2004), and Zhang et al. (2007). The total data set used for extracting the H_2O_t diffusivity expression in this study includes one experiment at 0.1 MPa (824 K), six experiments at about 0.1 GPa (834–911 K), two experiments at about 0.5 GPa (893–1708 K), and 11 experiments at about 1.0 GPa (786–1798 K). We recommend this new H_2O_t diffusivity expression for conditions of 786–1798 K, 0.01–8.0 wt.% H_2O_t, 0–1.0 GPa (including 0.1 MPa).

The correlation between $D_{H_2O_t}$ and temperature, pressure, and water content is illustrated in Fig. 7. $D_{H_2O_t}$ in-

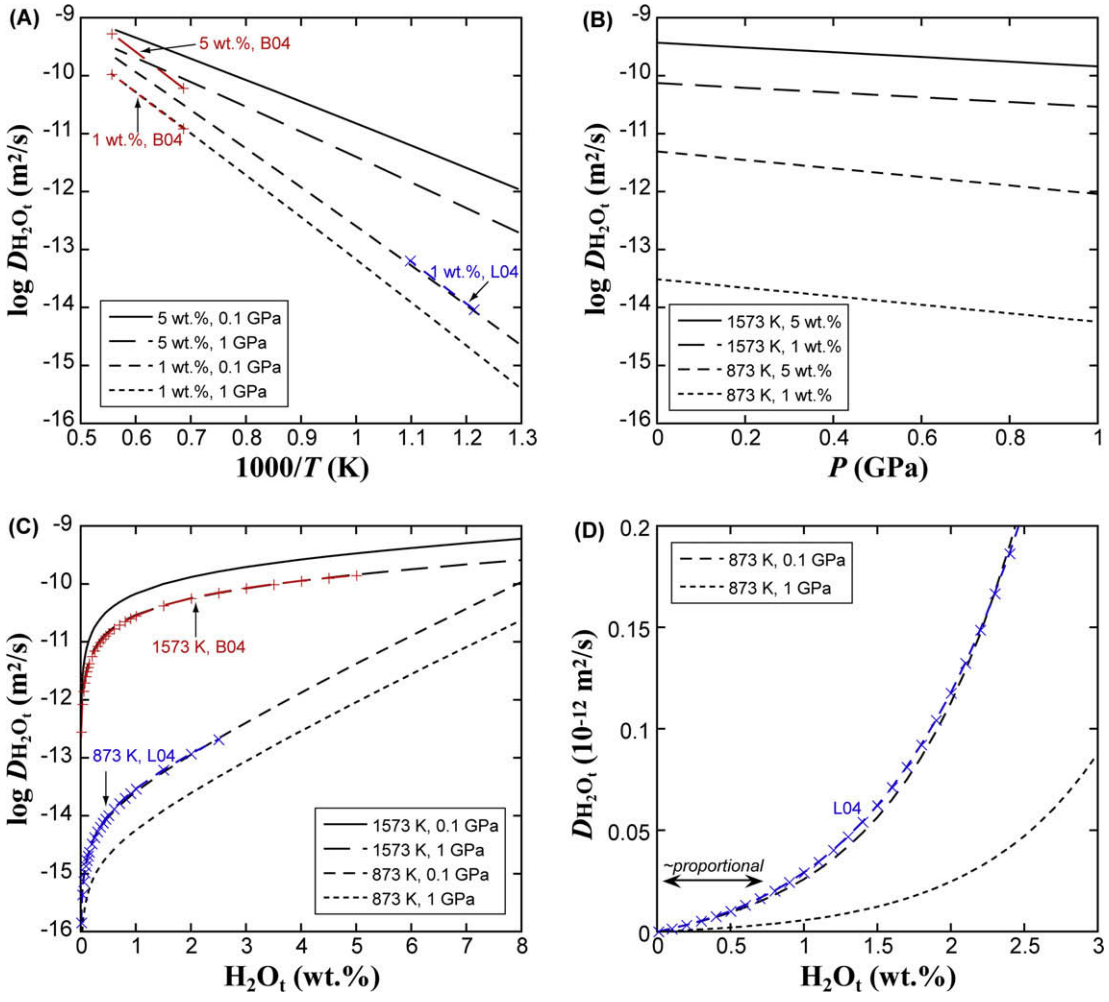

Fig. 7. Calculated H_2O_t diffusivity in dacite versus (A) temperature, (B) pressure, and (C and D) water content (Eq. (8)). Previous expressions from Liu et al. (2004a) in crosses and Behrens et al. (2004) in pluses, which are valid only under limited P-T-H_2O_t conditions, are also plotted for comparison. Note the different vertical scale in (D). The proportionality between diffusivity and water content at $H_2O_t < 0.7$ wt.% transits to exponential dependence towards higher H_2O_t.

creases with temperature following an Arrhenius manner, and the activation energy depends strongly on water content and weakly on pressure (Fig. 7A). For example, the calculated E_a at 0.1 GPa decreases from 129 kJ/mol for 1 wt.% H_2O_t to 72 kJ/mol for 5 wt.% H_2O_t, whereas E_a at 1 wt.% increases by only 11 kJ/mol from 0.1 to 1 GPa. The presence of water is expected to depolymerize the melt structure and to increase the ionic porosity of the melt, which would lower the energy barrier for H_2O diffusion. Pressure reduces diffusivity more noticeably at low temperatures, by a factor of ~6 at 786–893 K over 1 GPa interval (Fig. 7B). $D_{H_2O_t}$ also strongly depends on H_2O concentration, especially at low T where proportional correlation can only hold at most to ~0.7 wt.% (Fig. 7C and D). The dependence of $D_{H_2O_t}$ on H_2O_t is strongly curved in a $\log D_{H_2O_t}$ vs H_2O_t plot (Fig. 7C) because at low H_2O_t, $D_{H_2O_t}$ is roughly proportional to H_2O_t (Fig. 7D) whereas at high H_2O_t, $\log D_{H_2O_t}$ is roughly linear to H_2O_t.

Because H_2O diffusion is faster than the diffusion of most cations, bubbles are expected to grow more rapidly than crystals. On the other hand, H_2O diffusion is still not efficient for water migration over a large distance. For example, at 1273 K and 0.2 GPa, diffusion distance of water after 100 years is only 1.3 m even at a high water content of 6 wt.%. Convection is much more efficient in long-distance mass transfers and homogenization of magma chambers.

Okumura and Nakashima (2006) reported average diffusion-out H_2O diffusivity in dacitic glass. Their diffusivity from certain experiments (such as the runs at 665 and 675 °C) was probably underestimated due to the curvature in absorbance versus $t^{1/2}$ plots. For comparison, we extract new diffusion-out diffusivity from their original data by using only data with less than 20% dehydration, and then find $D_{H_2O_t}$ at 1 wt.% using the method described in Ni and Zhang (2008). Fig. 8 compares their results with our model and shows that there is general consistency (within a factor of 1.8, slightly larger than experimental and model uncertainty).

4.3. Comparison with H_2O diffusion in rhyolite

The P-T-H_2O_t dependences of H_2O diffusivity in dacite follow similar trends as those in rhyolite (Ni and Zhang, 2008), such as rapid increase with water concentration and negative pressure effect. Compared to rhyolite, H_2O_t diffusivity in dacite increases with water content more strongly at $T < 1313$ K but less strongly at $T > 1313$ K, as shown in the plot of parameter a vs. temperature (Fig. 9A). Furthermore, H_2O_t diffusivity in dacite shows a stronger dependence on temperature than in rhyolite. For example, at 0.1 GPa and 1 wt.% H_2O_t, the activation energy for H_2O_t diffusion in dacite is 129 kJ/mol, larger than that in rhyolite (84 kJ/mol, Ni and Zhang, 2008). The difference in E_a leads to a crossover of H_2O diffusivity at ~1253 K (Fig. 9B) below which $D_{H_2O_t}$ in dacite is smaller than in rhyolite. As pressure increases to 1.0 GPa, the crossover temperature increases to ~1323 K. Calculations show that when water content is below 5 wt.%, H_2O_t diffusion in dacite is always lower than that in rhyolite at <1173 K

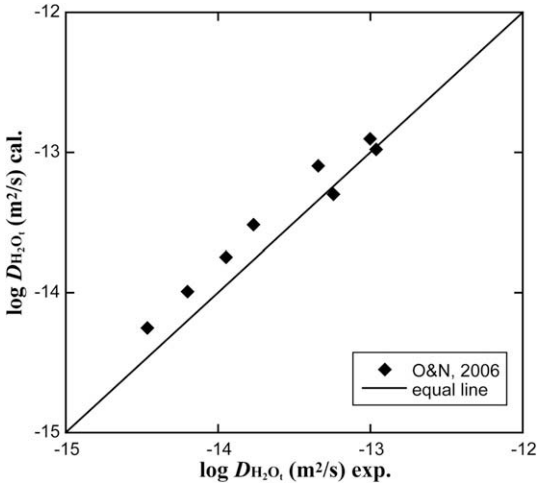

Fig. 8. Comparison of our new diffusivity expression with the in situ study of Okumura and Nakashima (2006). Average diffusion-out diffusivity is extracted from the data of Okumura and Nakashima (2006) where the glass still retains 80 percent of its initial water, and then converted to diffusivity at 1 wt.% H_2O concentration (see text for details).

(Fig. 9C) and faster than that in rhyolite at >1323 K. Diffusivity in both melts becomes very similar at $\geqslant 5$ wt.% H_2O_t, especially at 1.0 GPa (Fig. 9D). Pressure effect in rhyolite, about a factor of 10 per GPa at 800–900 K, is slightly larger than that in dacite.

Whittington et al. (2009) recently proposed a viscosity model for hydrous dacitic melts. By comparing with the viscosity of hydrous rhyolitic melts (Zhang et al., 2003), they found that at a given water content, the viscosity of hydrous dacite could become higher than that of hydrous rhyolite at T below ~950 K. Between hydrous dacite and hydrous rhyolite, the crossover temperature for melt viscosity is somewhat lower than that for H_2O diffusivity. Nonetheless, the general observation suggests a negative correlation between H_2O diffusivity and melt viscosity, which we further discuss below.

4.4. H_2O diffusivity and melt viscosity

The Einstein or Eyring relation (Einstein, 1905; Glasstone et al., 1941) predicts inverse proportionality between diffusivity (D) and viscosity (η):

$$D = \frac{kT}{\eta L} \tag{9}$$

where k is the Boltzmann constant, T is temperature, and L is characteristic length ($6\pi r$ for the Einstein relation and λ for the Eyring relation, with r being the radius of the diffusing particle, and λ being the jumping distance). The Einstein relation is derived for diffusion of neutral particles (such as noble gas molecules or H_2O molecules), and the Eyring relation is derived under the condition that viscous relaxation and diffusion are controlled by the same mechanism. The Einstein relation has been shown to be inapplicable to diffusion of neutral molecules in rhyolitic melts (e.g., Ni and Zhang, 2008; Wang et al., 2009), and it does not

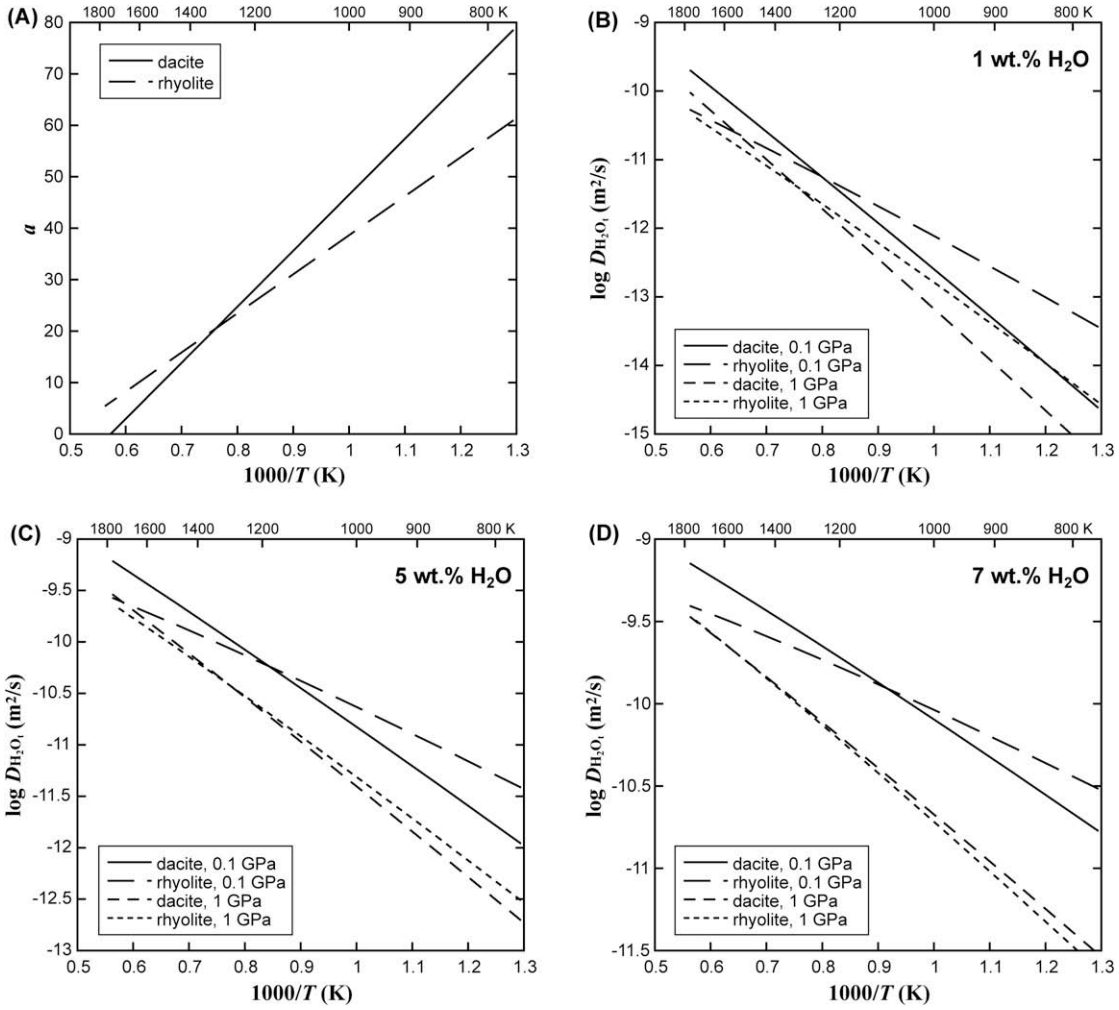

Fig. 9. Comparison of H_2O_t diffusivities in dacite (this study) and rhyolite (Ni and Zhang, 2008). (A) Parameter a; (B) $D_{H_2O_t}$ at 1 wt.% H_2O; (C) $D_{H_2O_t}$ at 5 wt.% H_2O; and (D) $D_{H_2O_m}$ at 7 wt.% H_2O. Note the difference in vertical scale of each plot. Crossover temperature of diffusivity in these two melts lies between 1173 and 1323 K at <5 wt.% H_2O_t.

apply to H_2O_m diffusion in dacitic melts either. The Einstein relation has also been shown to be inapplicable to ionic diffusion in silicate melts (e.g., Magaritz and Hofmann, 1978; Chakraborty, 1995), but the derivation of the Einstein relation means that it is not intended for ionic diffusion because attraction and repulsion forces between ions were not considered.

The Eyring relation has been found to hold well for oxygen and silicon self diffusion in anhydrous silicate melts (e.g., Shimizu and Kushiro, 1984; Tinker and Lesher, 2001). However, it does not hold for oxygen diffusion in hydrous melt (Behrens et al., 2007), or H_2O diffusion in rhyolite (Ni and Zhang, 2008) even though the curve shape of $\log D_{H_2O_t}$ vs H_2O_t content resembles that of $\log \eta$ vs H_2O_t (Fig. 7C). Note that it is inappropriate anyway to use either molecular H_2O diffusivity or total H_2O diffusivity to test the Eyring relation because it is unlikely that diffusion of H_2O and viscous flow have the same mechanism. For example, at 1000 K, H_2O_m diffusivity in dacite from this study changes by less than a factor of 2 from 0.01 wt.% to 0.5 wt.% water content, and H_2O_t diffusivity changes by almost two orders of magnitude, whereas the melt viscosity is lowered by more than four orders of magnitude over the same water content range based on Whittington et al. (2009). Therefore, as in rhyolite, H_2O_m diffusivity in dacite cannot be related to melt viscosity using the simple inverse correlation. The violation of the Eyring relation is due to the fact that viscosity is controlled by the diffusion of framework elements (such as Si, Al, and structual oxygen), not by other components (such as H_2O_m or the elements it contains).

4.5. Application to bubble growth in dacitic melt

Explosive volcanic eruptions are associated with the growth of H_2O (with some CO_2) bubbles inside melts under water-oversaturated conditions. Bubble growth is controlled by the slower of two dynamic-kinetic processes: viscous flow and water diffusion (Navon et al., 1998; Lensky et al., 2004). With established models of melt viscosity, water diffusivity and water solubility, the rate of bubble growth can be calculated (e.g., Proussevitch and Sahagian,

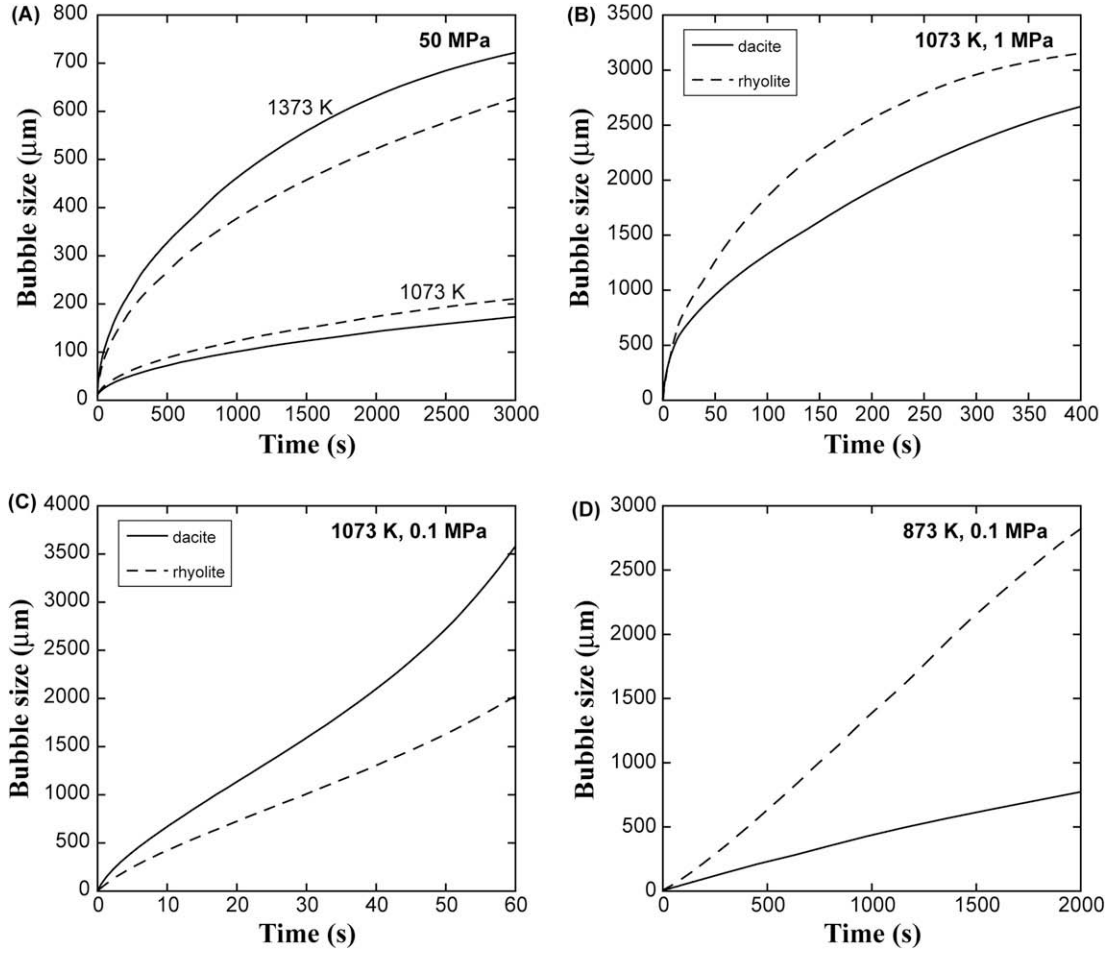

Fig. 10. Calculated bubble growth (initial bubble radius is 10 mm) in hydrous melts with 4 wt.% H_2O at (A) 50 MPa; (B) 1 MPa; and (C and D) 0.1 MPa using the model of Liu and Zhang (2000). H_2O solubility is from Zhang et al. (2007). For dacite, viscosity is from Whittington et al. (in press) and H_2O diffusivity is from this study. For rhyolite, viscosity is from Zhang et al. (2003) and H_2O diffusivity is from Ni and Zhang (2008).

1998) and compared with experimental observations (e.g., Liu and Zhang, 2000).

The new H_2O diffusivity expression in this study can be applied to simulate non-convective bubble growth in a melt with dacitic composition, using the viscosity model of Whittington et al. (2009) and the solubility model of Zhang et al. (2007). The bubble growth model is from Proussevitch and Sahagian (1998), as modified by Liu and Zhang (2000). Simulation results for hydrous melts with 4 wt.% H_2O are illustrated in Fig. 10. At a confining pressure of 50 MPa (in a volcanic conduit), H_2O concentration is relatively high in the melt shell surrounding the bubble, leading to low viscosity and rapid viscous relaxation. Hence, H_2O diffusion is the rate-determining process, and the growth curve is roughly parabolic. Bubble growth in dacite is faster at 1373 K but slower at 1073 K (Fig. 10A) than that in rhyolite due to their H_2O diffusivity crossover. At a lower confining pressure of 1 MPa, a bubble grows more rapidly than at 50 MPa (Fig. 10B), but the growth curve is still roughly parabolic (although less well defined than that at 50 MPa). At a confining pressure of 0.1 MPa (Fig. 10C and D), H_2O concentration in the melt adjacent to the bubble is very low, leading to high viscosity. Furthermore, lower pressure means the same amount of H_2O in the bubble leads to much more growth in bubble size, meaning more flow is necessary. Hence, bubble growth is controlled by viscosity, and the growth curve transits from parabolic to exponential. At these conditions bubble growth in dacite is faster than in rhyolite because the viscosity of dacite is lower than that of rhyolite by a factor of ~5 (Zhang et al., 2003; Whittington et al., 2009), although H_2O diffusion in dacite is slower. In a lava dome at 873 K and 0.1 MPa, the viscosity of rhyolite and dacite is very close, therefore bubble growth rate in rhyolite is faster again due to faster H_2O diffusion in rhyolite (Fig. 10D). Note that as a bubble grows even larger, diffusion gradually takes control of the growth until bubbles reach their equilibrium size (Navon et al., 1998; Lensky et al., 2004).

Bubble dissolution may be treated similarly. Degassed magma may be hydrated again through interaction with gas bubbles (Landi et al., 2008), which is essentially a bubble dissolution problem. With the diffusivity expression

from this study, the rate of melt hydration at various *P-T*-H_2O conditions can be evaluated. Because H_2O diffusivity strongly depends on water content, the hydration process becomes progressively more efficient as the melt uptakes more water.

5. CONCLUDING REMARKS

The experimental investigation on H_2O diffusion in dacite at 786–893 K and 0.48–0.95 GPa confirm that H_2O diffusivity increases rapidly with water concentration (at least up to 8 wt.% H_2O_t) in this temperature range. Our new data allow the examination of the strong Arrhenian temperature dependence of H_2O diffusivity at 1.0 GPa, as well as the pressure dependence of H_2O diffusivity at 800–900 K. Increasing pressure moderately slows the rate of diffusive transport of H_2O. Combined with previous studies under different *T–P* conditions, a general expression of H_2O diffusivity in dacitic melt is constructed. The new diffusivity expression can be applied to a variety of geological circumstances: 773–1773 K, 0–1 GPa, and 0.01–8 wt.% water content. Compared to rhyolite, H_2O diffusion in dacite shows a stronger dependence on temperature and water concentration, resulting in slower diffusion in dacite at $T < 1173$ K but more rapid diffusion at $T > 1323$ K than in rhyolite when $H_2O_t < 5$ wt.%. This study provides important data towards a universal H_2O diffusivity expression in felsic to basaltic calc-alkaline melts, and can be applied to both volcanic eruptions and deep-seated magmatic processes.

ACKNOWLEDGMENTS

We are grateful to Hejiu Hui and Yang Liu for synthesizing the dacitic glasses, Satoshi Okumura for providing the original dehydration data, Yang Chen for electron microprobe analysis, Eric Essene, Rebecca Lange, Zhan Chen, Sam Mukasa, and Haoyue Wang for discussion. Constructive reviews from Yan Liang, Oded Navon, and Alan Whittington significantly improved the manuscript. This work is supported by grants from NSF (EAR-0537598 and EAR-0711050).

REFERENCES

Behrens H. and Zhang Y. (2001) Ar diffusion in hydrous silicic melts implications for volatile diffusion mechanisms and fractionation. *Earth Planet. Sci. Lett.* **192**, 363–376.

Behrens, H. and Zhang, Y. (2009) H2O diffusion in peralkaline to eraluminous rhyolitic melts. *Contrib. Mineral. Petrol.* **157**, 765–780.

Behrens H. and Yamashita S. (2008) Water speciation in hydrous sodium tetrasilicate and hexasilicate melts: constraints from high temperature NIR spectroscopy. *Chem. Geol.* **256**, 306–315.

Behrens H., Zhang Y. and Xu Z. (2004) H_2O diffusion in dacitic and andesitic melts. *Geochim. Cosmochim. Acta* **68**, 5139–5150.

Behrens H., Zhang Y., Leschik M., Wiedenbeck M., Heide G. and Frischat G. H. (2007) Molecular H_2O as carrier for oxygen diffusion in hydrous silicate melts. *Earth Planet. Sci. Lett.* **254**, 69–76.

Bernard A., Demaiffe D., Mattielli N. and Punongbayan R. S. (1991) Anhydrite-bearing pumices from Mount Pinatubo: further evidence for the existence of sulphur-rich silicic magmas. *Nature* **354**, 139–140.

Bose K. and Ganguly J. (1995) Quartz-coesite transition revisited: reversed experimental determination at 500–1200 °C and retrieved thermochemical properties. *Am. Mineral.* **80**, 231–238.

Botcharnikov R. E., Behrens H. and Holtz F. (2006) Solubility and speciation of C–O–H fluids in andesitic melt at $T = 1100$–1300 °C and $P = 200$ and 500 MPa. *Chem. Geol.* **229**, 125–143.

Chakraborty S. (1995) Diffusion in silicate melts. *Rev. Mineral.* **32**, 411–503.

Chen C.-H., Depaolo D. J., Nakada S. and Shieh Y.-N. (1993) Relationship between eruption volume and neodymium isotopic composition at Unzen volcano. *Nature* **362**, 831–834.

Delaney J. R. and Karsten J. L. (1981) Ion microprobe studies of water in silicate melts: concentration-dependent water diffusion in obsidian. *Earth Planet. Sci. Lett.* **52**, 191–202.

Einstein A. (1905) The motion of small particles suspended in static liquids required by the molecular kinetic theory of heat. *Ann. Phys.* **17**, 549–560 (in German).

Freda C., Baker D. R., Romano C. and Scarlato P. (2003) Water diffusion in natural potassic melts. *Geol. Soc. Spec. Publ.* **213**, 53–62.

Fruchter J. S., Roberson D. E., Evans J. C., Olsen K. B., Lepel E. A., Laul J. C., Abel K. H., Sanders R. W., Jackson P. O., Wogman N. S., Perkins R. W., Van Tuyl H. H., Beauchamp R. H., Shade J. W., Daniel J. L., Erikson R. L., Sehmel G. A., Lee R. N., Robinson A. V., Moss O. R., Briant J. K. and Cannon W. C. (1980) Mount St. Helens ash from the 18 May 1980 eruption: chemical, physical, mineralogical, and biological properties. *Science* **209**, 1116–1125.

Ganguly J., Bhattacharya R. N. and Chakraborty S. (1988) Convolution effect in the determination of compositional profiles and diffusion coefficients by microprobe step scans. *Am. Mineral.* **73**, 901–909.

Glasstone S., Laidler K. J. and Eyring H. (1941) *The Theory of Rate Processes*. McGraw-Hill, New York, 611 pp.

Hui H., Zhang Y., Xu Z. and Behrens H. (2008) Pressure dependence of the speciation of dissolved H_2O in rhyolitic melts. *Geochim. Cosmochim. Acta* **72**, 3229–3240.

Landi P., Metrich N., Bertagnini A. and Rosi M. (2008) Recycling and "re-hydration" of degassed magma inducing transient dissolution/crystallization events at Stromboli (Italy). *J. Volcanol. Geotherm. Res.* **174**, 325–336.

Lensky N. G., Navon O. and Lyakhovsky V. (2004) Bubble growth during decompression of magma: experimental and theoretical investigation. *J. Volcanol. Geotherm. Res.* **129**, 7–22.

Liebske C., Behrens H., Holtz F. and Lange R. A. (2003) The influence of pressure and composition on the viscosity of andesitic melts. *Geochim. Cosmochim. Acta* **67**, 473–485.

Liu Y. and Zhang Y. (2000) Bubble growth in rhyolitic melt. *Earth Planet. Sci. Lett.* **181**, 251–264.

Liu Y., Zhang Y. and Behrens H. (2004a) H_2O diffusion in dacitic melts. *Chem. Geol.* **209**, 327–340.

Liu Y., Behrens H. and Zhang Y. (2004b) The speciation of dissolved H_2O in dacitic melt. *Am. Mineral.* **89**, 277–284.

Magaritz M. and Hofmann A. W. (1978) Diffusion of Sr, Ba and Na in obsidian. *Geochim. Cosmochim. Acta* **42**, 595–605.

Martel C., Dingwell D. B., Spieler O., Pichavant M. and Wilke M. (2000) Fragmentation of foamed silicic melts: an experimental study. *Earth Planet. Sci. Lett.* **178**, 47–58.

Navon O., Chekhmir A. and Lyakhovsky V. (1998) Bubble growth in highly viscous melts: theory, experiments and autoexplosivity of dome lavas. *Earth Planet. Sci. Lett.* **160**, 763–776.

Ni H. and Zhang Y. (2008) H_2O diffusion models in rhyolitic melt with new high pressure data. *Chem. Geol.* **250**, 68–78.

Ni H., Liu Y., Wang L. and Zhang Y. (2009) Water speciation and diffusion in haploandesitic melts at 743-873 K and 100 MPa. *Geochim. Cosmochim. Acta.* **73**, 3630–3641.

Nowak M. and Behrens H. (1997) An experimental investigation on diffusion of water in haplogranitic melts. *Contrib. Mineral. Petrol.* **126**, 365–376.

Ohlhorst S., Behrens H. and Holtz F. (2001) Compositional dependence of molar absorptivities of near-infrared OH- and H_2O bands in rhyolitic to basaltic glasses. *Chem. Geol.* **174**, 5–20.

Okumura S. and Nakashima S. (2004) Water diffusivity in rhyolitic glasses as determined by in situ IR spectrometry. *Phys. Chem. Miner.* **31**, 183–189.

Okumura S. and Nakashima S. (2006) Water diffusion in basaltic to dacitic glasses. *Chem. Geol.* **227**, 70–82.

Proussevitch A. A. and Sahagian D. L. (1998) Dynamics and energetics of bubble growth in magmas: analytical formulation and numerical modeling. *J. Geophys. Res.* **103**, 18223–18251.

Schuessler J. A., Botcharnikov R. E., Behrens H., Misiti V. and Freda C. (2008) Oxidation state of iron in hydrous phonotephritic melts. *Am. Mineral.* **93**, 1493–1504.

Shaw, H. R. (1974) Diffusion of H_2O in granitic liquids: I. Experimental data; II. Mass transfer in magma chambers. In *Geochemical Transport and Kinetics* (eds. A. W. Hofmann, B. J. Giletti, H. S. Yoder, and R. A. Yund). Carnegie Inst. Washington Publ., Washington, DC. pp. 139–170.

Shimizu N. and Kushiro I. (1984) Diffusivity of oxygen in jadeite and diopside melts at high pressures. *Geochim. Cosmochim. Acta* **48**, 1295–1303.

Silver L. A., Ihinger P. D. and Stolper E. M. (1990) The influence of bulk composition on the speciation of water in silicate glasses. *Contrib. Mineral. Petrol.* **104**, 142–162.

Tinker D. and Lesher C. E. (2001) Self diffusion of Si and O in dacitic liquid at high pressures. *Am. Mineral.* **86**, 1–13.

Szramek L., Gardner J. E. and Larsen J. (2006) Degassing and microlite crystallization of basaltic andesite magma erupting at Arenal Volcano, Costa Rica. *J. Volcanol. Geotherm. Res.* **157**, 182–201.

Wang, H., Xu, Z., Behrens, H. and Zhang, Y. (2009) Water diffusion in Mount Changbai peralkaline rhyolitic melt. *Contrib. Mineral. Petrol.*, doi:10.1007/s00410-009-0392-7.

Watson E. B. (1991) Diffusion of dissolved CO_2 and Cl in hydrous silicic to intermediate magmas. *Geochim. Cosmochim. Acta* **55**, 1897–1902.

Whittington, A. G., Hellwig, B. M., Behrens, H., Joachim, B., Stechern, A. and Vetere, F. (2009) The viscosity of hydours dacitic liquids: implications for the rheology of evolving silicic magmas. *Bul. Volcanol.* **71**, 185–199.

Withers A. C. and Behrens H. (1999) Temperature-induced changes in the NIR spectra of hydrous albitic and rhyolitic glasses between 300 and 100 K. *Phys. Chem. Minerals* **27**, 119–132.

Yamashita S., Kitamura T. and Kusakabe M. (1997) Infrared spectroscopy of hydrous glasses of arc magma compositions. *Geochem. J.* **31**, 169–174.

York D. (1966) Least-squares fitting of a straight line. *Can. J. Phys.* **44**, 1079–1086.

Zhang Y. (1999) A criterion for the fragmentation of bubbly magma based on brittle failure theory. *Nature* **402**, 648–650.

Zhang Y. and Behrens H. (2000) H_2O diffusion in rhyolitic melts and glasses. *Chem. Geol.* **169**, 243–262.

Zhang Y. and Stolper E. M. (1991) Water diffusion in a basaltic melt. *Nature* **351**, 306–309.

Zhang Y., Stolper E. M. and Wasserburg G. J. (1991) Diffusion of water in rhyolitic glasses. *Geochim. Cosmochim. Acta* **55**, 441–456.

Zhang Y., Belcher R., Ihinger P. D., Wang L., Xu Z. and Newman S. (1997) New calibration of infrared measurement of dissolved water in rhyolitic glasses. *Geochim. Cosmochim. Acta* **61**, 3089–3100.

Zhang Y., Xu Z. and Liu Y. (2003) Viscosity of hydrous rhyolitic melts inferred from kinetic experiments, and a new viscosity model. *Am. Mineral.* **88**, 1741–1752.

Zhang Y., Xu Z., Zhu M. and Wang H. (2007) Silicate melt properties and volcanic eruptions. *Rev. Geophys.* **45**, RG4004. doi:10.1029/2006RG000216.

Associate editor: F.J. Ryerson